ARTICLE IN PRESS

Nature Communications

https://doi.org/10.1038/s41467-026-73178-x

Article in Press

Mortise-and-tenon like van der Waals joints for strong and tough materials via multi-flow microfluidics

Received: 5 September 2025

Accepted: 30 April 2026

Cite this article as: Cai, G., Wang, Z., Li, P. *et al.* Mortise-and-tenon like van der Waals joints for strong and tough materials via multi-flow microfluidics. *Nat Commun* (2026). https://doi.org/10.1038/s41467-026-73178-x

Gangfeng Cai, Ziqiu Wang, Peng Li, Zihao Deng, Xin Ming, Lidan Wang, Kaiwen Li, Yingjun Liu, Weiwei Gao, Zhen Xu & Chao Gao

We are providing an unedited version of this manuscript to give early access to its findings. Before final publication, the manuscript will undergo further editing. Please note there may be errors present which affect the content, and all legal disclaimers apply.

If this paper is publishing under a Transparent Peer Review model then Peer Review reports will publish with the final article.

ARTICLE IN PRESS

© The Author(s) 2026. **Open Access** This article is licensed under a Creative Commons Attribution-NonCommercial-NoDerivatives 4.0 International License, which permits any non-commercial use, sharing, distribution and reproduction in any medium or format, as long as you give appropriate credit to the original author(s) and the source, provide a link to the Creative Commons licence, and indicate if you modified the licensed material. You do not have permission under this licence to share adapted material derived from this article or parts of it. The images or other third party material in this article are included in the article's Creative Commons licence, unless indicated otherwise in a credit line to the material. If material is not included in the article's Creative Commons licence and your intended use is not permitted by statutory regulation or exceeds the permitted use, you will need to obtain permission directly from the copyright holder. To view a copy of this licence, visit http://creativecommons.org/licenses/by-nc-nd/4.0/.

ARTICLE IN PRESS

TITLE

Mortise-and-tenon like van der Waals joints for strong and tough materials via multi-flow microfluidics

AUTHORS

Gangfeng Cai (蔡刚峰)[1†], Ziqiu Wang (王子秋) [1†], Peng Li (李鹏) [1*], Zihao Deng (邓子豪) [1], Xin Ming (明鑫) [1], Lidan Wang (王利丹) [1], Kaiwen Li (李楷文) [1], Yingjun Liu (刘英军) [1], Weiwei Gao (高微微) [1], Zhen Xu (许震) [1*], Chao Gao (高超) [1*]

[1] MOE Key Laboratory of Macromolecular Synthesis and Functionalization, Zhejiang Key Laboratory of Advanced Organic Materials and Technologies, International Research Center for X Polymers, Research Center for Advanced Fibers, Department of Polymer Science and Engineering, Zhejiang University, 866 Yuhangtang Rd, Hangzhou 310058, China.

[*]Corresponding authors: pengli512@zju.edu.cn (P. L.); zhenxu@zju.edu.cn (Z.X.); chaogao@zju.edu.cn (C.G.)

ARTICLE IN PRESS

ABSTRACT

The construction of anisotropic structures from their anisotropic building blocks across multiple length scales usually leads to unique properties of materials, such as nanowires and nanofilaments. However, two-dimensional nanosheets with distinct anisotropic topology are scarcely employed to engineer diverse anisotropic materials with desirable properties. Here, we report anisotropy-tailored graphene nanosheets with periodic arrangement in three-dimensional space, produced by multi-flow microfluidics. Upon film densification, a classical Chinese mortise-and-tenon like van der Walls joint architecture forms from such anisotropic tailored graphene nanosheets, enabling the resulting material to achieve a tensile strength of 2.11 gigapascal and an exceptional toughness of 87.44 megajoules per cubic meter. This philosophy of the multi-flow microfluidics controlling anisotropy-tailored graphene nanosheets and the mortise-and-tenon joint model should find use in the designing of structural materials.

ARTICLE IN PRESS

INTRODUCTION

Natural materials usually show a combination of normally exclusive properties, attributed to their hierarchically anisotropic structures across multiple length scale[1–4]. Such hierarchical structures are often constructed by regular arrangement of their anisotropic building blocks along varied directions in 3D space, enabling efficient load redistribution, damage tolerance, and multifunctional performance. Inspired by these natural anisotropic structures, several artificial materials were achieved to combine high strength and toughness, such as the enamel-inspired nanocomposites with anisotropic hydroxyapatite nanowires and the polymeric fibres with anisotropic nanofilaments[5,6].

Two-dimensional (2D) nanosheets, like graphene and graphene oxide (GO), are anisotropic building blocks with quite different in-plane and out-of-plane properties[7,8]. Specifically, Young's modulus of graphitic materials is 1060 GPa along the a-axis but only 36.5 GPa along the c-axis[9]. Macroscopic graphene films with anisotropic layered structure have been achieved by optimizing the high in-plane performance of such 2D building blocks, which pursuing highly aligned and near flat layer-structure with essentially homogeneous stacks of parallel nanosheets with a single z-director. The preparation and the mechanical response to their interlayer interaction and nanosheet orientation have been systematically understood in both experimental and modeling aspects[10–13]. For example, centrifugal casting and plastic-stretching minimized random wrinkles in films and promoted the alignment, yielding a high tensile strength of 0.66-1.3 GPa yet a decreased strain of 1-2%[12–15]. Aside from the anisotropic layer structure from 2D nanosheets with optimized stacking alignment, it remains a challenge to engineer or tailor anisotropic structures from such direction-specific 2D nanosheets especially with desirable properties, such as the combination of high strength and toughness. Bioinspired nacre structures were designed to achieve both high strength and toughness in graphene materials with layered structure by introducing secondary ductile phases as soft mortar[16–18]. Beyond the nacre-like brick-and-mortar model, tailoring the anisotropic assembly of direction-specific 2D nanosheets should represent a feasible way to create

ARTICLE IN PRESS

macroscopic materials with wondering properties like other anisotropic natural and artificial materials.

Herein, we achieve the anisotropic assembly of direction-specific 2D nanosheets in three-dimensional (3D) space via a multi-flow microfluidics (Supplementary Fig. 1). Using such a multi-flow microfluidics, we tailor the periodic distribution of GO nanosheets alternatively having x-, y-, and z-director in a hydrogel film. A Chinese classical mortise-and-tenon joint-like structure is formed in the densified film materials by the huge compressive deformation of x-director nanosheets into van der Waals (vdW) interlocks[19]. The graphene bulks from z-director nanosheets award the high in-plane strength, while the vdW joints from x-director nanosheets effectively dissipate deformation energy. By adjusting the graphene bulk size, joint content, and bulk-laying form, graphene materials behave from weak and brittle to strong yet brittle, weak yet ductile, and strong yet tough. This design concept not only simultaneously achieves the strengthening and toughening of materials from pure 2D inorganic nanosheets, but also proposes a mortise-and-tenon joint model in designing structural materials.

ARTICLE IN PRESS

RESULTS

Mortise-and-tenon like vdW joint via multi-flow microfluidics

Mortise-and-tenon joint is an ancient Chinese wooden architecture, where the joints between the pure wood are connected by mortise and tenon to form a flexible frame. It can not only withstand large loads, but allows certain movements and deformation, which make it offset the seismic energy and reduce the impact from earthquakes. Thus, the mortise-and-tenon joints are applied in most traditional buildings (Fig. 1a,b and Supplementary Fig. 2), such as the Yingxian wooden pagoda, known as the world's largest and oldest existing pure wooden pavilion building. We designed the anisotropic assembly of pure direction-specific 2D nanosheets, and then constructed mortise-and-tenon vdW joints in their densified film materials.

ARTICLE IN PRESS

The design concept of anisotropic assembly of direction-specific 2D nanosheets is shown in Fig. 1c-g. A flat 2D nanosheet is anisotropic with direction-specific director in 3D space. Direction-free isotropic vdW materials, such as graphene microsphere, were produced by randomly assembling 2D nanosheets without specific directors[20]. Direction-specific anisotropic vdW materials, such as graphene films, were prepared by orderly assembling 2D nanosheets with specific z-director (Fig. 1h and Supplementary Fig. 1). We design the direction-tailored anisotropic vdW materials by periodically distributing 2D GO nanosheets using a multi-flow microfluidics (Supplementary Fig. 3). Horizontal and vertical GO nanosheets with x- and z-director are generated by the shear flow of arrayed holes. The local expansion flow in a single arrayed hole directs the mildly vertical GO nanosheets with y-director as evidenced by computed tomography results (Supplementary Fig. 4 and Supplementary Video 1). In these cases, two or three specific directions of 2D GO nanosheets were successfully created in materials (x-y-z directors in Fig. 1e,g; y-z directors in Supplementary Fig. 5a,b; x-y directors in Supplementary Fig. 5c,d). Notably, such periodically distributed x-, y-, and z-director GO nanosheets were verified to form in the multi-flow microfluidics over a broad range of flow rates and GO concentrations, illustrating the multi-flow shear field is effectively stable for accurately construct such direction-tailored anisotropic graphene materials (Supplementary Fig. 6).

Macroscopic graphene films are produced after densifying these anisotropic GO hydrogels through solvent evaporation and chemical reduction using hydroiodic acid (also called rGO films, Supplementary Fig. 7). In such a typical film densification process, the horizontal graphene nanosheets with z-director are closely stacked, forming the aligned graphene bulks. In contrast, the vertically aligned x-director nanosheets experience huge deformation under unidirectional compression in the densification process. We conducted time-sequence tracking of the drying process of the hydrogel film, revealing that x-director nanosheets were severely inter-folded and inter-weaved in the huge deformation (Fig. 2a-c). The inter-folded nanosheets ultimately form the interlocked joints between neighboring graphene bulks. On the one hand, the interlocked vdW

ARTICLE IN PRESS

joints connect the adjacent strong and aligned graphene bulks robustly without easy separation. On the other hand, the incompact vdW joints, acting as weak interfaces, endow the material with certain deforming ability and flaw tolerance, effectively deflecting the crack propagation. Given the similar concept to the flexible mortise-and-tenon joint in Chinese woodworking, the interlocked joints in graphene films were named as mortise-and-tenon vdW joints (Fig. 2d).

Cross-sectional SEM image of solid GO film clearly visualizes these distinct alternating regions (Fig. 2d), highlighting the stark contrast between the dense, aligned nanosheet stacking within the bulks (Fig. 2e) and the interlocked yet incompact vdW joints (Fig. 2f,g). The densely packed and aligned graphene nanosheets in bulks afford load-bearing capacity by effective interlayer shearing[21,22]. The vdW joints separate the intact graphene film into individual bulks, effectively hindering potential sharp crack propagation. In short, tailoring the anisotropic assembly of 2D nanosheets presents a unique synergy that seamlessly constructs densely stacked graphene bulks and mortise-and-tenon vdW joints in the films, which is crucial for achieving designable properties in 2D materials, especially having simultaneously high strength and excellent toughness.

Designable performance of graphene films

By constructing mortise-and-tenon vdW joints from anisotropic assembly of 2D GO nanosheets, graphene films show distinct mechanical properties, typically varying by coding the bulk-laying forms, bulk size, and joint content. The four bulk structures and their corresponding fracture modes are illustrated in Fig. 3a. For clarity, the thickness and width of a single hole in arrayed multi-flow are labeled as h and w, respectively. H and W represent the thickness and width of an intact film channel, respectively. The (w, h) denotes the fabrication conditions of arrayed multi-flow (Fig. 3a and Supplementary Fig. 3b).

Traditional graphene film and control sample in this work should have the identical z-director graphene nanosheets. In this ideal mode, the intact film is constructed by densely stacked and aligned graphene nanosheets as a single bulk film. Thus, such a graphene film should display high strength and stiffness. However, random wrinkles often generate in graphene films during their

ARTICLE IN PRESS

solution processing, resulting in a lower strength[13,15]. The tensile strength of the control sample is 0.49 GPa (Fig. 3b). The bulk-laying structure in Mode 1 is constructed by horizontally arrayed multi-flow, leading to y- and z-director GO nanosheets. At fixed *W*, decreasing *h* enhances the shear-induced alignment of graphene nanosheets with z-director, thereby improving the nanosheet orientation of graphene films in Mode 1 (improved alignment from 0.80 to 0.93, Supplementary Fig. 8)[23]. The significantly improved orientation and dense stacking with removed microvoids contribute to the monotonically increased tensile strength with decreasing *h*, similar to previous reports where wrinkle minimization and improved alignment strengthen graphene films (Supplementary Fig. 9)[13,14]. The film (*W*, 100) shows improved strength (1.85 GPa), Young's modulus (57.7 GPa), but decreased strain (2.2%) and toughness (19.27 MJ/m^3, strong yet stiff behavior, Fig. 3b,c and Supplementary Fig. 10a-e).

Vertically arrayed multi-flow inversely directs the bulk structure with x- and y-director GO nanosheets, as shown in Supplementary Fig. 5c, d. As clearly evidenced in the structural tracking of drying process, x-director GO nanosheets seriously deform to mortise-and-tenon vdW joints (Fig. 2a-c), which make these graphene films in Mode 2 highly ductile (Fig. 3a). In our multi-flow microfluidic, the channel width *W* is divided into arrayed holes with single hole width of *w*, and x-director GO nanosheets (i. e., solid vdW joints) form at every width of *w*. Thus, the joint number across the film is $N_{joint} = W/w+1$. For clarity, we defined a normalized joint content as ~ 1/*w*, independent of the absolute sample width. With the increase of 1/*w*, the tensile strain and toughness are highly enhanced from 2.6% to 8.4% and from 7.29 MJ/m^3 to 29.4 MJ/m^3, with the slightly enhanced strength from 0.49 GPa to 0.72 GPa (weak yet ductile behavior, Fig. 3b,c, Supplementary Fig. 10f-j, and Fig. 11a). These results indicate that the joint content (1/*w*) is the primary structural parameter governing the toughening in our mortise-and-tenon vdW joints architecture.

Mode 3 and 4 combine the horizontally and vertically arrayed multi-flow to produce a bulk structure with synergistical x-, y-, and z-director GO nanosheets (Fig. 3a and Supplementary Fig. 4). Note, we focused on fabricating graphene films by fixing *h* as low as 100 μm, which efficiently

ARTICLE IN PRESS

aligns graphene nanosheets (reducing y-director GO nanosheets) and provides strong graphene bulks as evidenced in Mode 1 (Supplementary Fig. 8). This unique arrayed multi-flow divides the intact film into much more individual bulks (Supplementary Fig. 12). In Mode 3, with the decrease of *w*, increased joint content 1/*w* strongly toughens films (Supplementary Fig. 11b). The graphene film (100, 100) simultaneously shows a high tensile strength of 2.02 GPa, a large tensile strain of 7.6%, and an excellent toughness of 74.7 MJ/m^3 (strong yet tough behavior, Fig. 3b,c, Supplementary Fig. 10k-o, and Fig. 11b). Compared with the film (*W*, 100), the toughness is improved by around 280%. While comparing with the film (100, *H*), the tensile strength is reinforced by over 180%. Thus, the combination of strong individual bulks and flexible vdW joints awards graphene films synergistically improved strength and toughness. Given the anisotropic assembly of 2D graphene nanosheets, we also tested the anisotropic tensile properties of the films in Mode 3 (200, 100). Under vertical loading along x-director, the interlocked vdW joints become the weakest links between the graphene bulks. Consequently, fracture preferentially occurs along these weak joints, resulting in decreased strength and toughness (Supplementary Figs. 13 and 14).

Creatively, we interlaced the individual bulks of the graphene film (200, 100) like the brick arrangement in building house (Mode 4), showing a distinct bulk-laying form from Mode 3, as shown in Fig. 1f,g, and Fig. 3a. The interlaced bulks disrupt the otherwise continuous vdW joints, reasonably increasing the energy dissipation under deformation. Therefore, these films (200, 100) display further enhanced tensile strength of 2.11 GPa and toughness of 87.44 MJ/m^3, higher than those of the optimized (100, 100) films (Fig. 3b,c). Compared with the graphene films with the same bulk size (200, 100) yet without interlaced bulk-laying form, the tensile strength is improved by 17.9%, and the toughness is reinforced by 70.2% (Supplementary Fig. 15). Overall, we tailored the anisotropic assembly of 2D nanosheets in graphene materials like those anisotropic building blocks in natural materials, and achieved the designable mechanical properties of graphene films by constructing mortise-and-tenon vdW joints and coding the bulk-laying form, bulk size, and joint content (Supplementary Table 1).

ARTICLE IN PRESS

Strengthening while toughening

The optimized graphene film simultaneously shows a high tensile strength of 2.11 GPa and toughness of 87.44 MJ/m^3, 300-1000% higher than those of control sample. Densely stacked graphene bulks and mortise-and-tenon vdW joints are synergistically formed in the graphene film from periodically distributed z- and x-director GO nanosheets, respectively. These unique mortise-and-tenon vdW joints lead to their distinct properties of films. In a single dense and aligned graphene bulk, the efficient interlayer shearing from vdW forces between the overlapped graphene nanosheets leads to a high stress transfer efficiency, guaranteeing the high strength of the bulk. The incompact yet interlocked vdW joints endow the material with certain deforming ability, and effectively deflect the crack propagation[2] (Fig. 2). The combination of strong in-plane strength in each bulk and deflected crack propagation by mortise-and-tenon vdW joints, coming from the anisotropic assembly of 2D nanosheets, simultaneously strengthens and toughens graphene materials.

We *in situ* observed the fracture of the graphene film with mortise-and-tenon vdW joints in the presence of an initial notch (Fig. 4). When tension was applied, the initial crack propagated with obvious deflection, and a new microcrack appeared. The two cracks finally converged to rupture the film. In the entire fracturing process, crack deflection and rough surface were witnessed. The optical microscope and scanning electron microscopy (SEM) images of the fracture surfaces also demonstrate the discontinuous crack propagation at the vdW joints (Supplementary Fig. 16a). For deeply understanding the correlation between crack deflection and vdW joints, we further marked the typical crack deflection regions in the SEM images (Fig. 4d). It clearly shows that the crack deflection occurs at every width of ~127 μm, which is in accordance with the statistical width of z-director GO nanosheets in hydrogel films (~125 μm) and bulk size in solid films (~130 μm, Supplementary Fig. 17). On the contrary, the straight fracture surface of control sample illustrates its sharp crack propagation (Supplementary Fig. 16b).

The toughening mechanism was systematically analyzed. By restricting our choice of pure

ARTICLE IN PRESS

graphene constituents, most of the usual toughening mechanisms seen in ductile materials were excluded, such as dislocation plasticity or chain shearing. The extrinsic reinforcement comes from the anisotropic construction of the material and the load redistribution from the architecture of individual graphene bulks and vdW joints (Fig. 4a). Crack deflection, multiple cracking, crack bridging and branching at the crack tip, efficiently relieve the local high stresses[2,24]. The interlocked joints bridge the adjacent bulks, leading to efficient energy dissipation by frictional sliding during bulk pull-out, breaking of the joints (neighbor joints separate), and out-of-plane peeling[25], as demonstrated by the fracture tracking (Fig. 4b-e). Voids located at the joints also contribute by acting as local crack arresters by a Cook-Gordon mechanism[26] (Fig. 2g). With the nacre-like brick-and-mortar topology and stiffness ratio between two different brittle phases, previous work has achieved toughening in ceramics[24]. We constructed an architecture of mortise-and-tenon like vdW joints in 2D inorganic materials, reducing the stress concentration around the crack tip thanks to a more efficient load redistribution. The deformation is delocalized, and strain redistributes throughout the entire structure. These mechanisms could contribute to the high level of toughness achieved in these structures. The toughening structure of mortise-and-tenon like vdW joints is also consistent with established principles for bio-inspired architecture, where interface and size dictate flaw tolerance and extrinsic toughening[27–29].

Generality of the mortise-and-tenon like vdW joints

MXene is another typically anisotropic 2D nanosheet with interlayer vdW forces and could be solution-processed to high-performance macroscopic materials, like films[30–33]. Based on the design concept of anisotropic assembly of direction-specific 2D nanosheets, we also fabricated reinforced MXene-based films (100, 100) by constructing mortise-and-tenon like vdW joints. A small amount of GO nanosheets (10 wt%) were added to MXene solution for facile preparation, because the obtained MXene has too small lateral size to successfully prepare pure films by wet spinning (Supplementary Fig. 18). Such films show synergistically improved strength, strain, and toughness by 119%, 122%, and 511% compared with those of control films, respectively,

ARTICLE IN PRESS

illustrating the generality of the multi-flow microfluidics and the mortise-and-tenon vdW joints (Fig. 5a). The fracture section of the reinforced MXene-based film shows clear toughening evidences of discontinuous crack propagation and crack deflection at the crack tip around vdW joints, which is different from the sharp fracture of control sample[24] (Fig. 5b).

We concluded an Ashby chart of tensile strength and toughness for comparing the achieved films with previously reported materials (Fig. 5c and Supplementary Tables 2 and 3). Materials assembled by pure graphene nanosheets have significantly improved tensile strength via aligning graphene nanosheets[12,13,34]. Whereas the aligned graphene nanosheets enhance their tensile strength, yet awarding materials brittleness. The tensile strength reached 0.6-1.3 GPa, but the toughness was lower than 20 MJ/m^3. Nearly 40 MJ/m^3 toughness was efficiently achieved by introducing polymeric ductile phases into brick-and-mortar structures[16]. In this work, inspired by ancient Chinese mortise-and-tenon joints, we created a vdW joint architecture with single constituent of graphene, achieving a record-high average strength of 2.11 GPa and a toughness of 87.44 MJ/m^3, and significant improvements compared with those of most pure graphene materials. The toughness is also double that of graphene materials with classical brick-and-mortar structure by introducing polymeric mortar[16,22].

Because of the pure graphene constituent without polymeric phases, our chemically reduced graphene films show significant electrical conductivity of 1395-1489 S/cm, higher than that of previous reports of introducing polymeric mortar (Fig. 5d and Supplementary Fig. 19). High electrical conductivity renders excellent electromagnetic interference (EMI) shielding performance to these films (Fig. 5e). The EMI shielding effectiveness (EMI SE) of the film (3.4 μm) is about 40 dB at frequency ranging from 2-18 GHz, showing a remarkable improvement compared with that of the control film and a competitive performance to that of previously reported carbon-based films (Supplementary Fig. 20).

By alternatively stacking the films with mortise-and-tenon like vdW joints and thin epoxy resin,

ARTICLE IN PRESS

we fabricated pre-reinforced film-based layered composites (Supplementary Fig. 21). This layered composite shows a tensile strength of 1.75 GPa and a noteworthy toughness of 53.77 MJ/m^3, both overwhelming the pristine epoxy resin (Fig. 5f). These properties vary from the weight content of layered graphene films, being competitive with those of previously reported outstanding layer nanocomposites, metal foils, and even carbon fibre-based composites[13,35–38] (Supplementary Figs. 22 and 23 and Table 4). The fracture section displays a typical discontinuous crack propagation similar to that observed in natural nacre (Fig. 5f).

In this study, we achieved the anisotropic assembly of direction-specific 2D inorganic nanosheets, created a mortise-and-tenon like vdW joints architecture, and specifically produced synergistically strong and tough graphene films, MXene-based films, and pre-reinforced film layered composites. We foresee further broadening of the mortise-and-tenon joints in the development of strong and tough structural materials, lightweight metamaterials, and advanced composites for practical applications.

ARTICLE IN PRESS

METHODS

Materials

Aqueous GO dispersions were purchased from Hangzhou Gaoxi Technology Co. Ltd (www.gaoxitech.com). MXene solution ($Ti_3C_2T_x$) was purchased from XFNano Co. Ltd (Supplementary Fig. 18). Hydroiodic acid (HI) was purchased from Energy Chemical. Other reagents were purchased from Sinopharm Chemical Reagent Co., Ltd and used as received.

Preparation of spinning dope

GO spinning dope: Spinning dope of GO in N, N-dimethylformamide (DMF) was obtained by solvent exchange from an aqueous GO dispersion. Briefly, the aqueous GO dispersion was centrifuged at 6000 rpm/min for 30 min per cycle, the supernatant was removed, and the sediment was redispersed in DMF. This centrifugation and redispersion process was repeated at least five times until water was replaced by DMF. The resulting GO@DMF spinning dope was used to fabricate graphene films. Aqueous GO dispersion was purchased from

ARTICLE IN PRESS

Hangzhou Gaoxi Technology Co. Ltd (www.gaoxitech.com). The average lateral size of the GO is 10.4 μm.

MXene/GO spinning dope: The MXene/GO aqueous dispersion was prepared by mixing the MXene and GO dispersion with a mass ratio of 9:1.

Preparation of graphene films

The preparation of graphene films is based on our self-made wet-spinning method. Typically, GO@DMF or GO@H_2O liquid crystal spinning dope (0.8 wt%) was injected through the arrayed multi-flow microfluidics with (*w*, *h*) into the coagulation bath (mixture of ethyl acetate and dichloromethane or 3 wt% $CaCl_2$ solution). The as-spun hydrogel films exhibited anisotropic assembled GO nanosheets and were then dried to densified GO films. Followed by chemical reduction by the mixture of HI and ethanol (volume ratio of 1:3) in a tension state, graphene films with mortise-and-tenon like vdW joints were finally obtained. The control sample was fabricated by injecting GO liquid crystal solution through the intact wet-spinning channel (*W*, *H*) without arrayed multi-flow.

Preparation of the MXene-based composite film

The MXene-based composite film was obtained also by the same wet-spinning method with the arrayed multi-flow microfluidics. Briefly, MXene/GO aqueous spinning dope was extruded through the arrayed multi-flow microfluidics (100, 100). $CaCl_2$ solution (3 wt%) was used as the coagulation reagent and replaced by deionized water for at least 3 times. After drying the hydrogel film with anisotropic assembled nanosheets and chemically reducing the film by hydroiodic acid (HI) and ethanol (1:3), densified MXene-based film was obtained. The control sample was obtained with the same film-channel without the arrayed multi-flow.

Preparation of the graphene film/epoxy resin composite

Pre-reinforced graphene films and epoxy resin films were alternately stacked on a Teflon plate to construct a layered architecture (Supplementary Fig. 21). The amount of graphene film and epoxy resin was adjusted to obtain composites containing 85 wt%, 70 wt% and 55 wt% graphene films. The stacked assembly was then transferred to a hot press and compressed at 10 MPa and 80 °C for 12 h, allowing consolidation of the layered structure and curing of the epoxy resin. After cooling to room temperature, the resulting composite was removed from the Teflon plate and cut into the desired dimensions for subsequent characterization.

ARTICLE IN PRESS

Tests of films and composites

Stress-strain curves of films were obtained by testing rectangular strips of the fabricated films (2 mm width and 10 mm length) with a mechanical tester Instron 2344 at a tensile rate of 5 mm min^{-1}. The width of the strip sample was verified again by polarized optical microscopy (POM, Nikon, E600POL) images and the thickness was measured by SEM image following most literatures. Five specimens were tested for each sample. The toughness of all samples was determined by the fracture energy (integrated area of the stress-strain curve). The Young's modulus was determined by the slope of the linear region of the stress-strain curves. The electrical conductivity is measured by a standard four-probe method on an electrical transport properties measurement system composing a Keithley 2460 source meter.

Characterization of the fracture

The fracture process of the graphene film with an initial notch was tracked *in situ* by SEM (Carl Zeiss, EVO 10) equipped with a tensile stage (PI, M-112.2DG1). During *in situ* observation, the sample was imaged at an accelerating voltage of 5 kV. The fracture surfaces of samples after tensile testing were collected by SEM using the same instrument at an accelerating voltage of 5 kV. Before SEM observation, the samples were blown with nitrogen, mounted on conductive carbon tape, and examined without conductive coating.

Characterization of the direction-tailored GO nanosheets in hydrogel films

The hydrogel film was freeze-dried to aerogel film, which was used for characterizing the distribution of GO nanosheets by SEM and microcomputed tomography (μCT, Carl Zeiss, 520 Versa). The mortise-and-tenon like vdW joints and individual graphene bulks were verified by SEM and transmission electron microscope (TEM, FEI Tecnai, G2 F20) operated at 300 kV. TEM samples were prepared by focused ion beam technology (FEI, Quanta 3D FEG).

Calculation of the orientation

The alignment of graphene nanosheets is characterized by wide-angle X-ray scattering (WAXS, Shanghai Synchrotron Radiation Facility, BL16B1, wavelength 0.124 nm, Supplementary Tables 5). The azimuthal scan of the (002) reflection in 2D WAXS patterns give the Herman orientation factor[13,32].

The orientation order was quantified by converting the orientation distribution into Herman's orientation

ARTICLE IN PRESS

function, *f*, defined as:

$$f = < \frac{3}{2} cos^2\varphi - \frac{1}{2} > \quad (1)$$

where φ is azimuthal distribution, and $cos^2\varphi$ is the average value of the square of the cosine of angle φ.

$$cos^2\varphi = \frac{\int_0^{\frac{\pi}{2}} I(\varphi) cos^2\varphi sin\varphi d\varphi}{\int_0^{\frac{\pi}{2}} I(\varphi) sin\varphi d\varphi} \quad (2)$$

where, $I(\varphi)$ is the intensity at φ in the azimuthal scanning curve.

DATA AVAILABILITY

All data that support the findings of this study are presented in the manuscript and Supplementary Information. Source data are provided with this paper.

REFERENCES

1. Wegst, U. G. K., Bai, H., Saiz, E., Tomsia, A. P. & Ritchie, R. O. Bioinspired structural materials. *Nat. Mater.* **14**, 23–36 (2015).
2. Ritchie, R. O. The conflicts between strength and toughness. *Nat. Mater.* **10**, 817–822 (2011).
3. Tirrell, D. A. Putting a new spin on spider silk. *Science* **271**, 39–40 (1996).
4. Mao, L. B. *et al.* Synthetic nacre by predesigned matrix-directed mineralization. *Science* **354**, 107–110 (2016).
5. Zhao, H. *et al.* Multiscale engineered artificial tooth enamel. *Science* **375**, 551–556 (2022).
6. Liao, X. *et al.* High strength in combination with high toughness in robust and sustainable polymeric materials. *Science* **366**, 1376–1379 (2019).
7. Geim, A. K. Graphene: status and prospects. *Science* **324**, 1530–1534 (2009).
8. Novoselov, K. S. *et al.* Electric field effect in atomically thin carbon films. *Science* **306**, 666–669 (2004).
9. Huang, X. Fabrication and properties of carbon fibers. *Materials* **2**, 2369–2403 (2009).
10. Compton, O. C. *et al.* Tuning the mechanical properties of graphene oxide paper and its associated polymer nanocomposites by controlling cooperative intersheet hydrogen bonding. *ACS Nano* **6**, 2008–2019 (2012).
11. Sen, D., Novoselov, K. S., Reis, P. M. & Buehler, M. J. Tearing graphene sheets from adhesive substrates produces tapered nanoribbons. *Small* **6**, 1108–1116 (2010).
12. Zhong, J. *et al.* Efficient and scalable synthesis of highly aligned and compact two-dimensional nanosheet films with record performances. *Nat. Commun.* **9**, 3484 (2018).
13. Li, P. *et al.* Continuous crystalline graphene papers with gigapascal strength by intercalation modulated plasticization. *Nat. Commun.* **11**, 2645 (2020).

ARTICLE IN PRESS

ARTICLE IN PRESS

14. Shen, K. *et al.* Intercalated oligomer doubles plasticity for strong and conductive graphene papers and composites. *Carbon* **208**, 160–169 (2023).
15. Lin, J. *et al.* The origin of the sheet size predicament in graphene macroscopic papers. *ACS Nano* **15**, 4824–4832 (2021).
16. Wan, S. *et al.* High-strength scalable graphene sheets by freezing stretch-induced alignment. *Nat. Mater.* **20**, 624–631 (2021).
17. Wan, S., Xu, F., Jiang, L. & Cheng, Q. Superior fatigue resistant bioinspired graphene-based nanocomposite via synergistic interfacial interactions. *Adv. Funct. Mater.* **27**, 1605636 (2017).
18. Gong, S., Jiang, L. & Cheng, Q. Robust bioinspired graphene-based nanocomposites via synergistic toughening of zinc ions and covalent bonding. *J. Mater. Chem. A* **4**, 17073–17079 (2016).
19. Chang, D. *et al.* Reversible fusion and fission of graphene oxide-based fibers. *Science* **372**, 614–617 (2021).
20. Zhao, X., Yao, W., Gao, W., Chen, H. & Gao, C. Wet-spun superelastic graphene aerogel millispheres with group effect. *Adv. Mater.* **29**, 1701482 (2017).
21. Gong, L. *et al.* Interfacial stress transfer in a graphene monolayer nanocomposite. *Adv. Mater.* **22**, 2694–2697 (2010).
22. Yang, J. *et al.* Water-induced strong isotropic MXene-bridged graphene sheets for electrochemical energy storage. *Science* **383**, 771–777 (2024).
23. Zhao, C. *et al.* Layered nanocomposites by shear-flow-induced alignment of nanosheets. *Nature* **580**, 210–215 (2020).
24. Bouville, F. *et al.* Strong, tough and stiff bioinspired ceramics from brittle constituents. *Nat. Mater.* **13**, 508–514 (2014).
25. Zhang, X. *et al.* Carbon nanotube fibers with dynamic strength up to 14 GPa. *Science* **384**, 1318–1323 (2024).
26. Cook, J. *et al.* A mechanism for the control of crack propagation in all-brittle systems. *Proc. R. Soc. Lond. Ser. Math. Phys. Sci.* **282**, 508–520 (1964).
27. Gao, H., Ji, B., Jäger, I. L., Arzt, E. & Fratzl, P. Materials become insensitive to flaws at nanoscale: Lessons from nature. *Proc. Natl. Acad. Sci.* **100**, 5597–5600 (2003).
28. Espinosa, H. D., Rim, J. E., Barthelat, F. & Buehler, M. J. Merger of structure and material in nacre and bone – Perspectives on *de novo* biomimetic materials. *Prog. Mater. Sci.* **54**, 1059–1100 (2009).
29. Meyers, M. A., McKittrick, J. & Chen, P.-Y. Structural biological materials: critical mechanics-materials connections. *Science* **339**, 773–779 (2013).
30. Shahzad, F. *et al.* Electromagnetic interference shielding with 2D transition metal carbides (MXenes). *Science* **353**, 1137–1140 (2016).
31. Wan, S. *et al.* High-strength scalable MXene films through bridging-induced densification. *Science* **374**, 96–99 (2021).
32. Li, W. *et al.* Ultrastrong MXene film induced by sequential bridging with liquid metal. *Science*

ARTICLE IN PRESS

385, 62–68 (2024).
33. Zhang, J. *et al.* Scalable manufacturing of free-standing, strong $Ti_3C_2T_x$ MXene films with outstanding conductivity. *Adv. Mater.* **32**, 2001093 (2020).
34. Xin, G. *et al.* Microfluidics-enabled orientation and microstructure control of macroscopic graphene fibres. *Nat. Nanotechnol.* **14**, 168–175 (2019).
35. Podsiadlo, P. *et al.* Ultrastrong and stiff layered polymer nanocomposites. *Science* **318**, 80–83 (2007).
36. Zhu, J., Zhang, H. & Kotov, N. A. Thermodynamic and structural insights into nanocomposites engineering by comparing two materials assembly techniques for graphene. *ACS Nano* **7**, 4818–4829 (2013).
37. Walther, A. *et al.* Large-Area, Lightweight and thick biomimetic composites with superior material properties via fast, economic, and green pathways. *Nano Lett.* **10**, 2742–2748 (2010).
38. Putz, K. W., Compton, O. C., Palmeri, M. J., Nguyen, S. T. & Brinson, L. C. High-nanofiller-content graphene oxide–polymer nanocomposites via vacuum-assisted self-assembly. *Adv. Funct. Mater.* **20**, 3322–3329 (2010).
39. Zhang, M. *et al.* Multifunctional pristine chemically modified graphene films as strong as stainless steel. *Adv. Mater.* **27**, 6708–6713 (2015).
40. Li, W., Weng, C., Yang, W., Shen, L. & Bao, N. High-strength reduced graphene oxide paper prepared by a simple and efficient method. *J. Mater. Sci.* **56**, 14084–14095 (2021).
41. Chen, H., Müller, M. B., Gilmore, K. J., Wallace, G. G. & Li, D. Mechanically strong, electrically conductive, and biocompatible graphene paper. *Adv. Mater.* **20**, 3557–3561 (2008).
42. Zhang, Q., Wan, S., Jiang, L. & Cheng, Q. Bioinspired robust nanocomposites of cooper ions and hydroxypropyl cellulose synergistic toughening graphene oxide. *Sci. China Technol. Sci.* **60**, 758–764 (2017).
43. Wan, S. *et al.* Nacre-inspired integrated strong and tough reduced graphene oxide–poly(acrylic acid) nanocomposites. *Nanoscale* **8**, 5649–5656 (2016).
44. Hu, K. *et al.* Written-in conductive patterns on robust graphene oxide biopaper by electrochemical microstamping. *Angew. Chem. Int. Ed.* **52**, 13784–13788 (2013).
45. Gong, S., Zhang, Q., Wang, R., Jiang, L. & Cheng, Q. Synergistically toughening nacre-like graphene nanocomposites via gel-film transformation. *J. Mater. Chem. A* **5**, 16386–16392 (2017).
46. Li, Y. Q., Yu, T., Yang, T. Y., Zheng, L. X. & Liao, K. Bio-inspired nacre-like composite films based on graphene with superior mechanical, electrical, and biocompatible properties. *Adv. Mater.* **24**, 3426–3431 (2012).
47. Ni, H. *et al.* Robust bioinspired graphene film via π–π cross-linking. *ACS Appl. Mater. Interfaces* **9**, 24987–24992 (2017).
48. Ye, S., Chen, B., Hu, D., Liu, C. & Feng, J. Graphene-based films with integrated strength and toughness via a novel two-step method combining gel casting and surface crosslinking. *ChemNanoMat* **2**, 816–821 (2016).
49. Xu, Y., Bai, H., Lu, G., Li, C. & Shi, G. Flexible graphene films via the filtration of water-

ARTICLE IN PRESS

soluble noncovalent functionalized graphene sheets. *J. Am. Chem. Soc.* **130**, 5856–5857 (2008).
50. Wan, S. *et al.* Ultrastrong graphene films via long-chain π-bridging. *Matter* **1**, 389–401 (2019).
51. Cheng, Q., Wu, M., Li, M., Jiang, L. & Tang, Z. Ultratough artificial nacre based on conjugated cross-linked graphene oxide. *Angew. Chem. Int. Ed.* **52**, 3750–3755 (2013).
52. Cui, W. *et al.* A strong integrated strength and toughness artificial nacre based on dopamine cross-linked graphene oxide. *ACS Nano* **8**, 9511–9517 (2014).
53. Wan, S. *et al.* Fatigue resistant bioinspired composite from synergistic two-dimensional nanocomponents. *ACS Nano* **11**, 7074–7083 (2017).
54. Duan, J. *et al.* Bioinspired ternary artificial nacre nanocomposites based on reduced graphene oxide and nanofibrillar cellulose. *ACS Appl. Mater. Interfaces* **8**, 10545–10550 (2016).
55. Ming, P. *et al.* Nacre-inspired integrated nanocomposites with fire retardant properties by graphene oxide and montmorillonite. *J. Mater. Chem. A* **3**, 21194–21200 (2015).
56. Xiong, R. *et al.* Ultrarobust transparent cellulose nanocrystal-graphene membranes with high electrical conductivity. *Adv. Mater.* **28**, 1501–1509 (2016).
57. Gong, S. *et al.* Integrated ternary bioinspired nanocomposites via synergistic toughening of reduced graphene oxide and double-walled carbon nanotubes. *ACS Nano* **9**, 11568–11573 (2015).
58. Wen, Y., Wu, M., Zhang, M., Li, C. & Shi, G. Topological design of ultrastrong and highly conductive graphene films. *Adv. Mater.* **29**, 1702831 (2017).
59. Wan, S. *et al.* Synergistic toughening of graphene oxide–molybdenum disulfide–thermoplastic polyurethane ternary artificial nacre. *ACS Nano* **9**, 708–714 (2015).
60. Zhang, M., Huang, L., Chen, J., Li, C. & Shi, G. Ultratough, ultrastrong, and highly conductive graphene films with arbitrary sizes. *Adv. Mater.* **26**, 7588–7592 (2014).
61. Wan, S. *et al.* Use of synergistic interactions to fabricate strong, tough, and conductive artificial nacre based on graphene oxide and chitosan. *ACS Nano* **9**, 9830–9836 (2015).
62. Wan, S., Fang, S., Jiang, L., Cheng, Q. & Baughman, R. H. Strong, conductive, foldable graphene sheets by sequential ionic and π bridging. *Adv. Mater.* **30**, 1802733 (2018).
63. Wan, S. *et al.* Sequentially bridged graphene sheets with high strength, toughness, and electrical conductivity. *Proc. Natl. Acad. Sci.* **115**, 5359–5364 (2018).
64. Wang, L. *et al.* Superior strong and tough nacre-inspired materials by interlayer entanglement. *Nano Lett.* **23**, 3352–3361 (2023).
65. Ling, Z. *et al.* Flexible and conductive MXene films and nanocomposites with high capacitance. *Proc. Natl. Acad. Sci.* **111**, 16676–16681 (2014).
66. Liu, J. *et al.* Ultrastrong and highly conductive MXene-based films for high-performance electromagnetic interference shielding. *Adv. Electron. Mater.* **6**, 1901094 (2020).
67. Chen, H. *et al.* Pristine titanium carbide MXene films with environmentally stable conductivity and superior mechanical strength. *Adv. Funct. Mater.* **30**, 1906996 (2020).
68. Liu, Z. *et al.* Electrically conductive aluminum ion-reinforced MXene films for efficient electromagnetic interference shielding. *J. Mater. Chem. C* **8**, 1673–1678 (2020).
69. Liu, R. *et al.* Ultrathin biomimetic polymeric $Ti_3C_2T_x$ MXene composite films for

ARTICLE IN PRESS

electromagnetic interference shielding. *ACS Appl. Mater. Interfaces* **10**, 44787–44795 (2018).
70. Hu, C. *et al.* Characteristics of $Ti_3C_2T_x$–chitosan films with enhanced mechanical properties. *Front. Energy Res.* **4**, (2017).
71. Cao, W. T. *et al.* Binary strengthening and toughening of MXene/cellulose nanofiber composite paper with nacre-inspired structure and superior electromagnetic interference shielding properties. *ACS Nano* **12**, 4583–4593 (2018).
72. Tian, W. *et al.* Multifunctional nanocomposites with high strength and capacitance using 2D MXene and 1D nanocellulose. *Adv. Mater.* **31**, 1902977 (2019).
73. Zhan, Z., Song, Q., Zhou, Z. & Lu, C. Ultrastrong and conductive MXene/cellulose nanofiber films enhanced by hierarchical nano-architecture and interfacial interaction for flexible electromagnetic interference shielding. *J. Mater. Chem. C* **7**, 9820–9829 (2019).
74. Xie, F. *et al.* Ultrathin MXene/aramid nanofiber composite paper with excellent mechanical properties for efficient electromagnetic interference shielding. *Nanoscale* **11**, 23382–23391 (2019).
75. Weng, G. M. *et al.* Layer-by-layer assembly of cross-functional semi-transparent MXene-carbon nanotubes composite films for next-generation electromagnetic interference shielding. *Adv. Funct. Mater.* **28**, 1803360 (2018).
76. Lipton, J. *et al.* Mechanically strong and electrically conductive multilayer MXene nanocomposites. *Nanoscale* **11**, 20295–20300 (2019).
77. Wan, S. *et al.* Strong sequentially bridged MXene sheets. *Proc. Natl. Acad. Sci.* **117**, 27154–27161 (2020).
78. Lee, G. S. *et al.* Mussel inspired highly aligned $Ti_3C_2T_x$ MXene film with synergistic enhancement of mechanical strength and ambient stability. *ACS Nano* **14**, 11722–11732 (2020).
79. Wan, S. *et al.* Scalable ultrastrong MXene films with superior osteogenesis. *Nature* **634**, 1103–1110 (2024).

ARTICLE IN PRESS

ACKNOWLEDGEMENTS

We thank the members of staffs at Shanghai Synchrotron Radiation Facility for assistance in WAXS characterizations and the International Research Centre for X polymers. This work is supported by National Key Research and Development Program of China (2022YFA1205300, 2022YFA1205301) (Z. X.), the National Natural Science Foundation of China (52403051 (P. L. 52272046 (Y. L.)), the Natural Science Foundation of Zhejiang Province (LQN25E030008 (P. L.), LR23E020003 (Y. L.)), the Fundamental Research Funds for the Central Universities (226-2024-00074 (Z. X.), 226-2025-00219 (Y. L.)), Hundred Talents Program of Zhejiang University (188020*194231701/113) (Y. L.), Pioneer and Leading Goose R&D Program of Zhejiang (2026C02A1055 (Y. L.), 2023C01190 (Z. X.)).

ARTICLE IN PRESS

AUTHOR CONTRIBUTIONS STATEMENT

G. C. and Z. W. contributed equally to this work. P. L. contributed to the initiating idea. G. C. and Z. W. performed the experiments. K. L. helped to characterize the fracture. Z. D., X. M., L. W., Y. L., Z. X., and W. G. participated the discussion of mechanical behaviours. P. L., G. C., and C. G. wrote the manuscript. All authors commented on the manuscript.

COMPETING INTERESTS STATEMENT

The authors declare no competing interests.

ARTICLE IN PRESS

ARTICLE IN PRESS

Fig. 1 | Concept of the anisotropic assembly of 2D nanosheets and the densified mortise-and-tenon like vdW joints. a, Photograph of the Qiushi Lecture Hall at Zhejiang University built with mortise-and-tenon joints (Photo credit: Gangfeng Cai). **b,** Photograph of a mortise-and-tenon wooden joint model, showing the flexible but robust junction. **c,** Schematic illustrating the direction-specific 2D nanosheets in 3D space. **d-g**, Schematics and SEM images depicting the anisotropic assembly concept to design x- and z-director arranged 2D nanosheets in 3D space. **h**, Schematic illustration of the mortise-and-tenon vdW joint between aligned graphene bulks in solid graphene films after densifying the anisotropic assembled hydrogel films. Scale bars, 50 mm (b), 100 μm (e and g). The SEM experiments in e and g were independently repeated three times with similar results.

Fig. 2 | Formation of mortise-and-tenon-like vdW joints during drying. a-c, Time-sequence SEM images (top) and corresponding schematics (bottom) illustrating the x-director GO nanosheets in the huge deformation are inter-folded and inter-weaved to form the vdW joints. **d**, Cross-sectional SEM image of GO film, displaying alternating regions of aligned graphene bulks and mortise-and-tenon like vdW joints. **e**, TEM image of the graphene bulk, showing the dense stacking of GO nanosheets. **f**, High-magnification SEM images of the vdW joint region. **g**, TEM image of the vdW joint, with dashed lines and arrows indicating the interlocking interfaces and microvoids. Scale bars, 50 μm (a-c), 10 μm (d), 10 nm (e), 100 nm (inset of e), 5 μm (f), 5 nm (g), 50 nm (inset of g). The SEM and TEM experiments were independently repeated three times with similar results.

Fig. 3 | Designable mechanical properties of graphene films densified from anisotropic assembly of nanosheets. a, Schematic showing four bulk structures with varied anisotropic assembled graphene nanosheets and their potential fracture paths, in which Mode 1, 2, 3, and 4

ARTICLE IN PRESS

shows the film structures prepared from horizontally arrayed multi-flow (Supplementary Fig. 5b), vertically arrayed multi-flow (Supplementary Fig. 5d), horizontally and vertically arrayed multi-flow with (Fig. 1g) or without (Fig. 1e) interlaced bulk-laying forms, respectively. The horizontal and vertical sticks represent the graphene nanosheets with z- and x-directors, respectively. The dotted yellow line depicts the basic repetitive unit of anisotropic graphene nanosheets from a single hole. *W* and *H* denote the whole width and thickness of the intact film channel, respectively, *w* and *h* denote the width and thickness of a single hole in the arrayed multi-flow, respectively. The red lines indicate the varied fracture paths in each mode. **b**, Tensile stress-strain curves of graphene films with the varied anisotropic assembled graphene nanosheets. **c**, Mechanical properties of graphene films, including high strength (Mode 1), high ductility (Mode 2), and a combination of high strength and excellent toughness (Mode 3 and 4). Data in c are represented as mean values ± one standard deviation for independent samples ($n = 5$). Source data are provided as a Source Data file.

ARTICLE IN PRESS

ARTICLE IN PRESS

Fig. 4 | Strengthening and toughening mechanism of the graphene film constructed with mortise-and-tenon vdW joints. a, Schematic illustrating the toughening mechanism across multiple length scales. The aligned graphene bulks provide high in-plane strength, whereas the mortise-and-tenon vdW joints redistribute local stress and promote extrinsic toughening through crack deflection, multiple cracking, crack branching, frictional sliding, bulk pull-out, joint separation and out-of-plane peeling. **b-e**, SEM images of *in situ* tracking the fracture process of the graphene film with an initial notch. The fracture process shows discontinuous crack propagation with evident crack deflection, the formation of a new microcrack, and the eventual convergence of cracks to final failure. Typical crack deflection regions are highlighted by yellow dotted lines, indicating a crack deflection length (L_d) of ~127 μm, which agrees well with the statistical width of z-director GO nanosheets in the hydrogel films (~125 μm) and the bulk size in the solid films (~130 μm, Supplementary Fig. 17). Scale bars: 400 μm (b-e, top), 200 μm (b-e, bottom). The SEM experiments in b-e were independently repeated three times with similar results.

Fig. 5 | Generality of the mortise-and-tenon vdW joints. a, Tensile stress-strain curves of toughening MXene-based films (100, 100) and traditional films. **b**, SEM images of the typical fracture surfaces of toughening MXene-based films (left) and traditional films (right). Crack deflection regions near the vdW joints in the toughening MXene-based film indicate the extrinsic toughening mechanism, while the smooth fracture depicts the brittle breakage in traditional films. **c**, Ashby chart for comparing tensile strength and toughness of the graphene films and MXene-based films with mortise-and-tenon vdW joints (red/orange points) with those of reported graphene materials by aligning graphene nanosheets (blue hollow points) and introducing polymeric mortar (composites, blue filled points), MXene-based materials (green hollow points), and strong MXene-based composites by filling polymer mortar (green filled points) [12–15,17,18,22,31–33,39–79]. **d**, Electrical conductivity of the graphene films. **e**, Electromagnetic interference shielding effectiveness of the

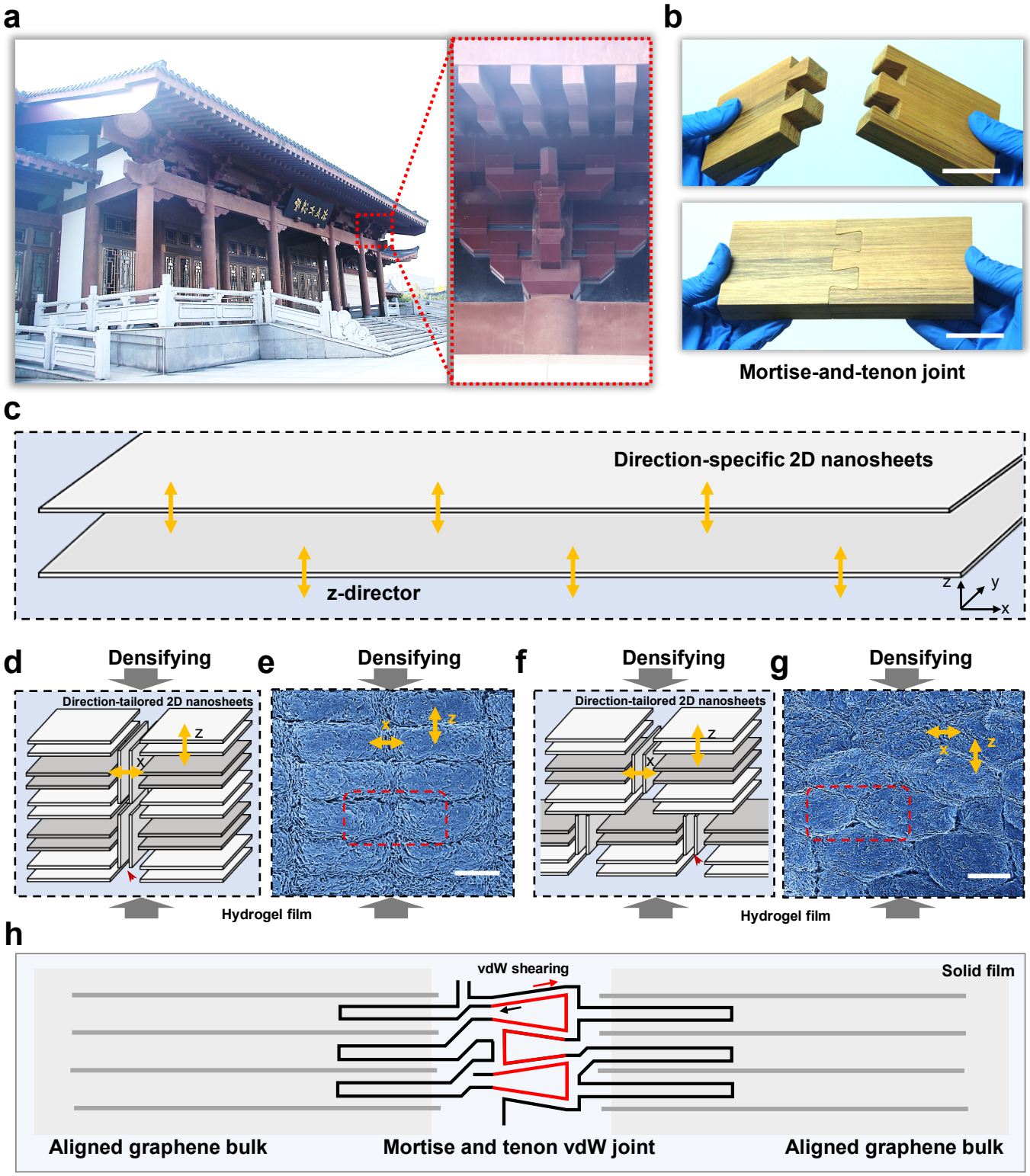
ARTICLE IN PRESS

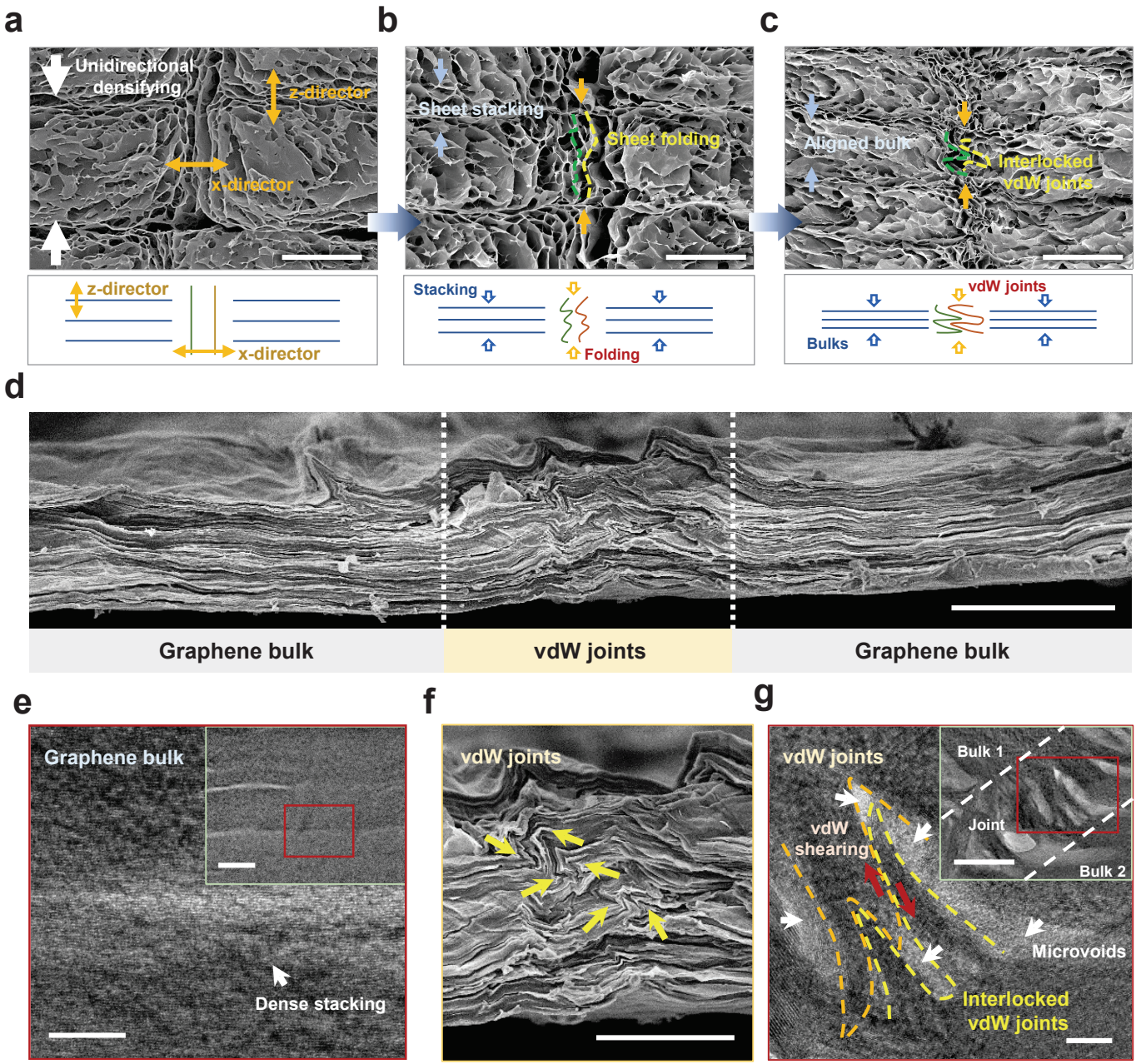
graphene films. **f**, Tensile stress-strain curves of the pre-reinforced film/epoxy resin layered composites with 85 wt% (red line), 70 wt% (blue line), and 55 wt% (gray line) graphene films. The inserts are the schematic of the layered composites (top) and the SEM image of the fracture section of a composite (down). Scale bars: 20 μm (top left of b), 10 μm (top right of b), 10 μm (bottom left of b), 5 μm (bottom right of b), 10 μm (f). SEM experiments in b were independently repeated three times with similar results. Data in d are represented as mean values ± one standard deviation for independent samples ($n = 5$). Source data are provided as a Source Data file.

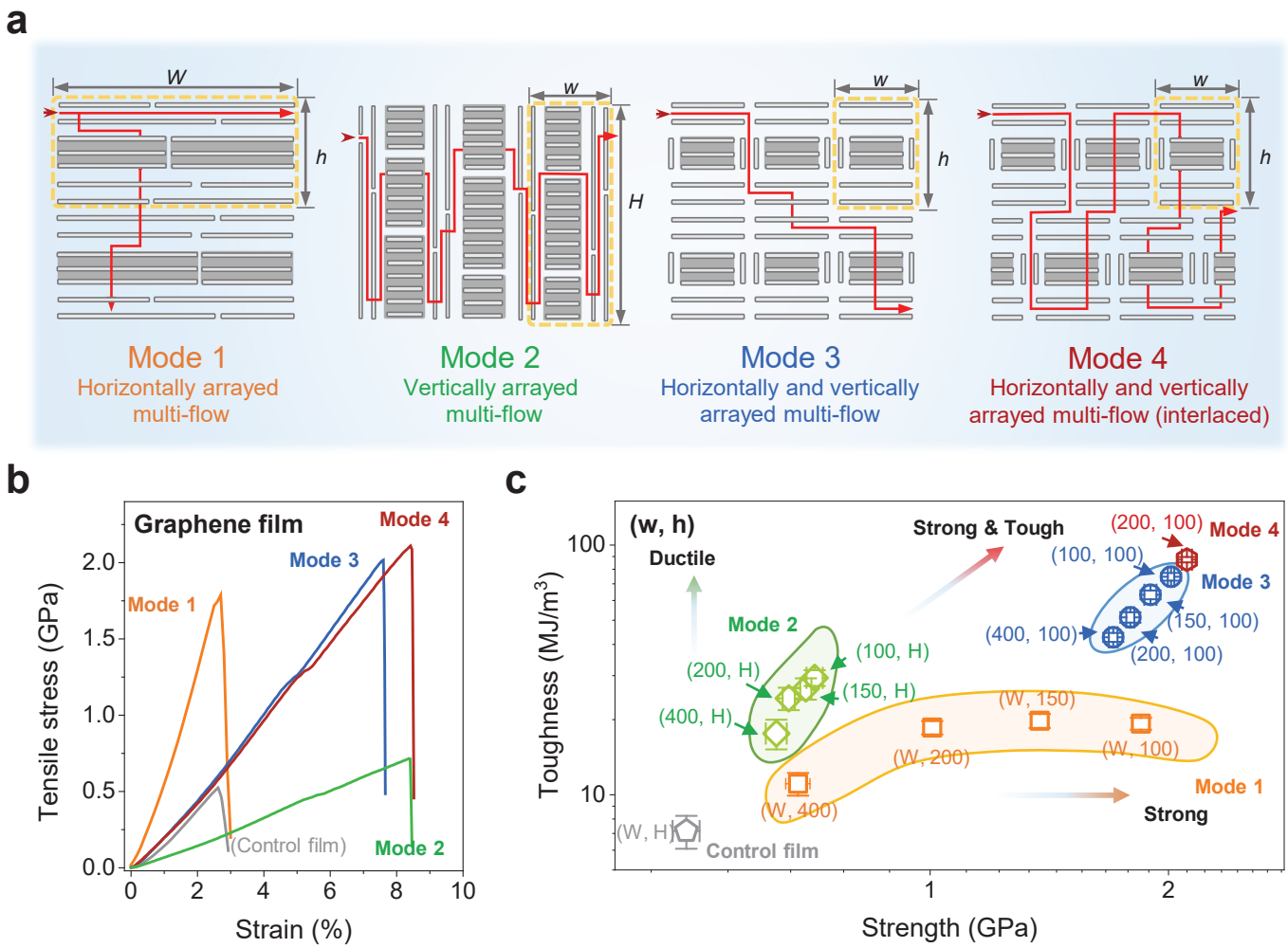
ARTICLE IN PRESS

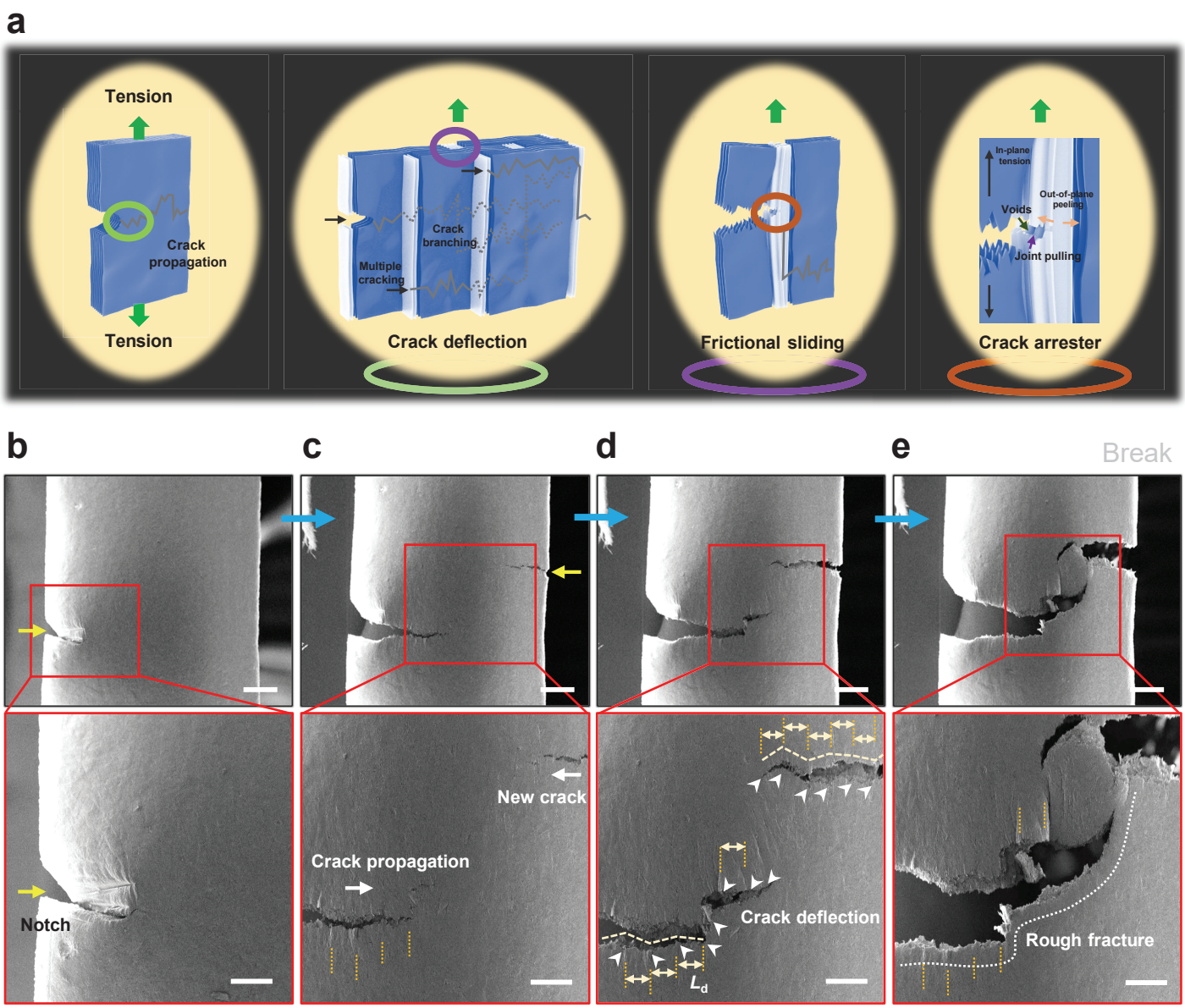
Editorial Summary:
Control of the arrangement of anisotropic units allows for control of properties. Authors achieve direction tailoring of 2D anisotropic sheets by multiflow technique, offering a mortise-and-tenon-like vdW joint model for strengthening and toughening in graphene

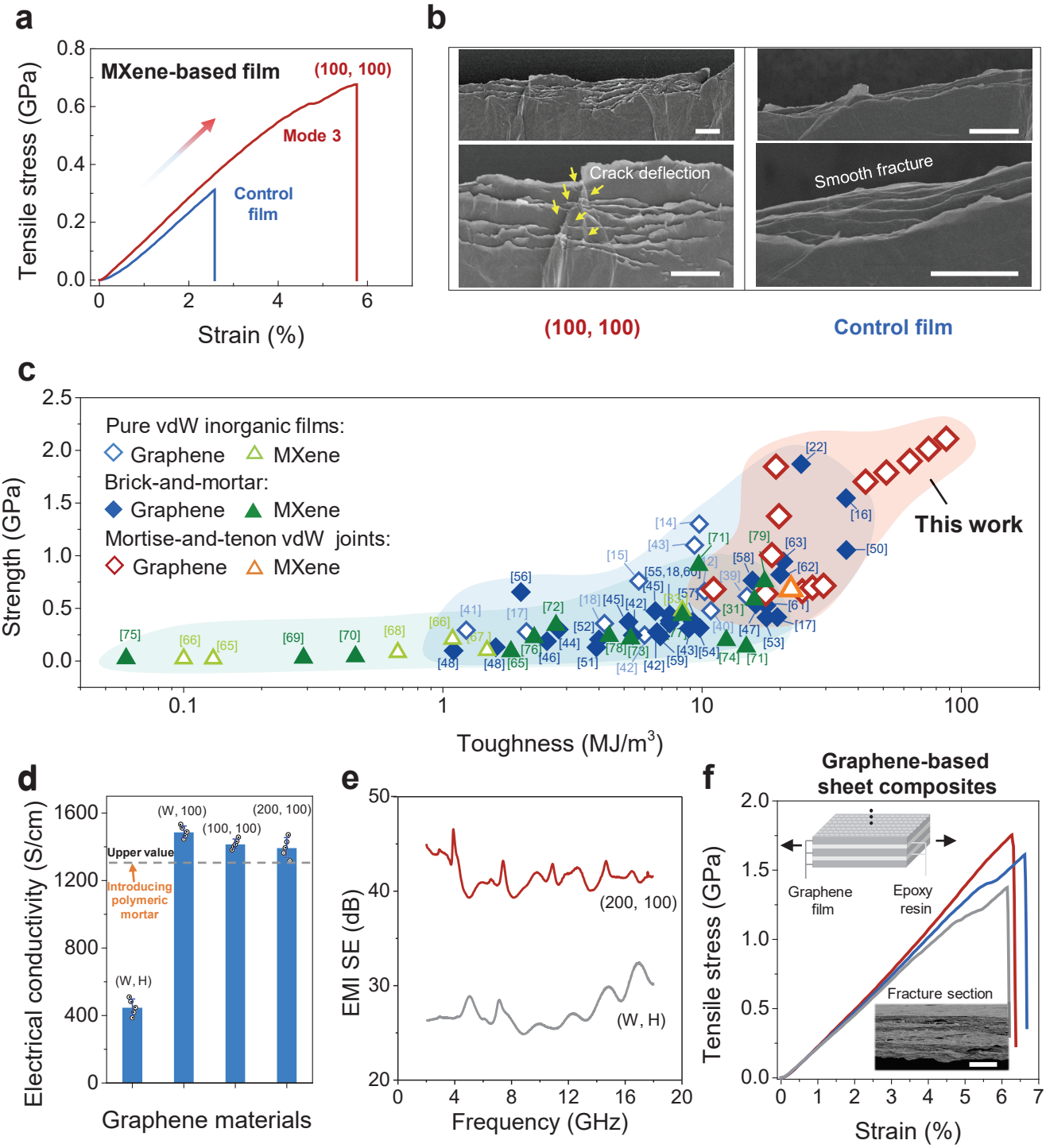
Peer review information: *Nature Communications* thanks the anonymous reviewers for their contribution to the peer review of this work. A peer review file is available.


a
b
Mortise-and-tenon joint
c
Direction-specific 2D nanosheets
z-director
z
y
x
d
Densifying
Direction-tailored 2D nanosheets
z
x
Hydrogel film
e
Densifying
x
z
f
Densifying
Direction-tailored 2D nanosheets
z
x
Hydrogel film
g
Densifying
x
z
h
vdW shearing
Solid film
Aligned graphene bulk
Mortise and tenon vdW joint
Aligned graphene bulk


a
b
c
Unidirectional densifying
z-director
x-director
Sheet stacking
Sheet folding
Aligned bulk
Interlocked vdW joints
z-director
x-director
Stacking
Folding
vdW joints
Bulks
d
Graphene bulk
vdW joints
Graphene bulk
e
Graphene bulk
Dense stacking
f
vdW joints
g
vdW joints
Bulk 1
Joint
Bulk 2
vdW shearing
Microvoids
Interlocked vdW joints


a
W
h
w
H
w
h
w
h
Mode 1
Horizontally arrayed multi-flow
Mode 2
Vertically arrayed multi-flow
Mode 3
Horizontally and vertically arrayed multi-flow
Mode 4
Horizontally and vertically arrayed multi-flow (interlaced)
b
Graphene film
Mode 4
Mode 3
Mode 1
(Control film)
Mode 2
Tensile stress (GPa)
Strain (%)
c
(w, h)
Ductile
Strong & Tough
Mode 4
(200, 100)
(100, 100)
Mode 3
(150, 100)
(400, 100)
(200, 100)
Mode 2
(100, H)
(200, H)
(150, H)
(400, H)
(W, 150)
(W, 200)
(W, 100)
Mode 1
Strong
(W, 400)
(W, H)
Control film
Toughness (MJ/m3)
Strength (GPa)


a
Tension
Crack propagation
Tension
Crack branching
Multiple cracking
Crack deflection
Frictional sliding
In-plane tension
Out-of-plane peeling
Voids
Joint pulling
Crack arrester
b
c
d
e
Break
Notch
New crack
Crack propagation
Crack deflection
L_d
Rough fracture


a
MXene-based film
(100, 100)
Mode 3
Control film
Tensile stress (GPa)
Strain (%)
b
Crack deflection
Smooth fracture
(100, 100)
Control film
c
Pure vdW inorganic films:
Graphene
MXene
Brick-and-mortar:
Graphene
MXene
Mortise-and-tenon vdW joints:
Graphene
MXene
This work
Strength (GPa)
Toughness (MJ/m3)
d
Upper value
Introducing polymeric mortar
(W, H)
(W, 100)
(100, 100)
(200, 100)
Electrical conductivity (S/cm)
Graphene materials
e
(200, 100)
(W, H)
EMI SE (dB)
Frequency (GHz)
f
Graphene-based sheet composites
Graphene film
Epoxy resin
Fracture section
Tensile stress (GPa)
Strain (%)